Application of Spherical Harmonics to the Modeling of Anatomical Shapes

P. Haigron[1], G. Lefaix[1], X. Riot[2], R. Collorec[1]

[1] Laboratoire Traitement du Signal et de l'Image, INSERM, Université de Rennes 1, Bât. 22, Campus de Beaulieu, 35042 Rennes Cedex, France.
[2] Société Hexale Technologies, PIBS, CP 33, 56038, Vannes, France.

3D shape modeling is a key issue in the resolution of major medical imaging problems. In this paper we address the problem of the modeling of closed free form anatomical shapes with spherical harmonics. We define the basis of an ongoing project by illustrating, through two preliminary applications, the interest of such a modeling. After the presentation of spherical harmonics, both for static modeling and for time-dependent modeling, applications to the modeling and deformation analysis of the vertebra shape from CT data, and to the modeling of the endocardial surface from SPECT data are successively depicted.

Keywords: 3D shape modeling, free form surfaces, spherical harmonics, time-dependent representation, deformation analysis, scoliotic spine, endocardial surface

Introduction

The two last decades have brought major advances in medical imaging. Today, the emergence and constant improvement of computed tomography, magnetic resonance imaging, nuclear imaging and other observation techniques, allow us to image structures and functions in three dimensions (3D). These new resources convey new obligations: the concern is less to produce aesthetic pictures of the anatomy (as it has been seen in visualization) than to design efficient health care procedures [Coatrieux, 96]. Some of the major issues in medical imaging are generic and can be seen as belonging to computer vision and graphics, others specifically feature the medical field and the requirements to deal with: image sensing, free form objects, low contrast tissues, time varying properties and moving (deformable) structures on the one hand, and reliability and real time constraints inherent to diagnosis and therapy objectives on the other. Diagnosis is the first objective. In addition to the availability of observations, it relies on our capability to extract, quantify and interpret the underlying information to discriminate the diseases.

In this context, 3D shape modeling has to deal with specific features such as: free form surfaces that cannot easily be decomposed into simple geometric primitives (they range from smooth surfaces to complex shaped topologies); significant inter-individual variations with time-varying properties at local as well as global levels; large spectrum of abnormal states (or diseases) that can greatly modify tissue properties and shapes or produce large deformations of organ subparts; complex motions and deformations, on both normal and abnormal cases, on which little prior knowledge is available. In return, 3D shape modeling is a key issue in the resolution of major medical imaging problems such as: the characterization and quantification of anatomical shape features; the 3D reconstruction when the clinical protocols require the acquisition of only a few of 2D images; the registration of multiple views of the objects, or multimodal observations, each corresponding to a given parameter describing structural properties or functional behaviors; the materialization of anatomical structures of interest in surgical procedures assuming that the basic rule consists in avoiding any damage to other structures.

This paper addresses the problem of the modeling of closed free form anatomical shapes with spherical harmonics. Spherical harmonics are

global functions that belong to the class of surface harmonics, they have interesting features for medical applications. Spherical harmonics constitute a basis of orthogonal functions, on which any finite energy and differentiable function can be expressed as a linear combination of the basis functions. Moreover, the accuracy of the modeling is arbitrarily defined by the level of decomposition. In other words, the details of a given shape are obtained by the highest level harmonics. This paper defines the basis of an ongoing project by illustrating, through two preliminary applications, the interest of such a modeling. After the presentation of spherical harmonics, both for static modeling and for time-dependent modeling, applications to the modeling and deformation analysis of the vertebra shape, and to the modeling of the heart left ventricle (from clinical data) are successively depicted.

3D Shape Modeling with Spherical Harmonics

Techniques of shape modeling have been greatly studied. A good review is given in [Bolle, 91]. The distinction between all the approaches can be established according to some key criteria, such as shape visualization, deformation, registration, characterization and classification. The data describing the shape can be object-centered or viewer-centered, and expressed in a cartesian, spherical or other coordinate systems. Regularity and sparseness of shape sampling depends on the acquisition device and on the efficiency of segmentation algorithms. One can also distinguish volume from surface models, both of which can be expressed in discrete or analytical forms. For instance, shape models based on voxels or octree constitute discrete volume representations. When it comes to analytical surface modeling, three kinds of representation are formally considered, i.e., parametric, implicit and explicit forms. Global representation uses a single functional form to describe the surface as a whole, whereas a piecewise representation is based on locally defined functions that are given in a parametric form. An example of piecewise representation can be found in [Sequeira, 92], where free form patches with polynomial functions are used to model vascular shapes. Global explicit representation forms can be illustrated by thin plate splines [Bookstein, 89]. Concerning global implicit functions, one can mention quadric surfaces, that are widely used for object representation purposes, and superquadrics [Solina, 90][Bardinet, 96] which can be deformed in different ways, including tapering, bending and making cavities. Nevertheless, superquadrics meet some difficulties in modeling complex shapes. Deformable models based on superquadrics [McInerney, 96] have been used to model and to characterize the shape and motion of the cardiac left ventricle [Pentland, 91]. Furthermore, hierarchical representations have been presented in the literature to model surfaces in a multiresolution scheme. Significant examples include: the multiresolution analysis used, both for data compression and for data visualization with radiosity techniques [DeRose, 95]; the spherical wavelets in geophysics problems [Freeden, 95]; and also surface harmonics which have recently been used in medical applications such as heart ventricle modeling [Matheny, 95][Chen, 94], anatomical shape registration and characterization [Burel, 95a][Burel, 95b]. Hierarchical approaches also combine several types of representations such as spherical harmonics and superquadrics or spherical wavelets and spherical harmonics.

Although, below, we consider the particular case of spherical harmonics, other coordinate systems can be employed depending on the shape to be modeled. Harmonic functions thus have been expressed in cylindrical, spheroidal, hyperspherical, spheroconal and spherical coordinate systems. Spherical harmonics are solutions of Laplace's equation expressed in a spherical coordinate system (Figure 1). These solutions are noted Y_l^m and are related to associated Legendre polynomials (appendix a.1 and a.2). This definition excludes the possibility of the radius r, from the center O to a surface point M, being multiple-valued [Max, 88]. The case of an object surface described by a non-starlike set of points will be discussed below, with the vertebra shape modeling. Furthermore, r is a function $r(\theta, \varphi)$ of θ and φ that is not necessarily continuous.

Spherical harmonics, belonging to the class of surface harmonics, have interesting properties for surface modeling [Matheny, 95], such as:

$$\begin{aligned} x &= r \cdot \sin\theta \cdot \cos\varphi, \\ y &= r \cdot \sin\theta \cdot \sin\varphi, \\ z &= r \cdot \cos\theta, \\ &\text{with} \quad 0 \le \theta \le \pi, \\ &\text{and} \quad 0 \le \varphi \le 2\pi. \end{aligned}$$

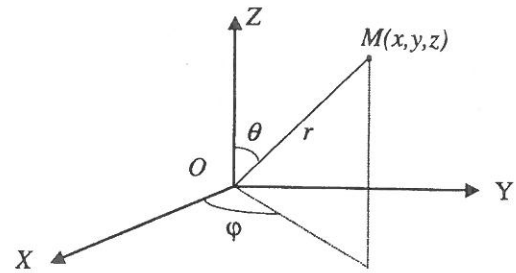

Fig. 1. Convention used for the spherical coordinate system.

- Orthogonality. The Y_l^m constitute the basis of orthogonal functions. This property assures uniqueness of the decomposition with respect to the integration over the sphere.
- Ordered in spatial frequency. This notion expresses a hierarchical decomposition of the shape. The accuracy of the modeling is arbitrarily defined by the level of decomposition L, i.e., the details of a given shape are obtained by the highest level harmonics.
- Completeness. Any finite energy and differentiable function defined on the sphere can be approximated by a linear combination of spherical harmonics:

$$\Psi(\theta, \varphi) = \sum_{l=0}^{\infty} \sum_{m=-l}^{l} C_l^m \cdot Y_l^m(\theta, \varphi), \quad (1)$$

where $\Psi(\theta, \varphi)$ is the surface and C_l^m are the coordinates of the shape on the spherical harmonics basis. The C_l^m coefficients are obtained by the projection of the shape onto the basis of the Y_l^m:

$$\begin{aligned} C_l^m &= \langle Y_l^m | \Psi \rangle \\ &= \int_0^{2\pi} d\varphi \int_0^{\pi} \sin\theta \cdot Y_l^m(\theta, \varphi) \Psi(\theta, \varphi) \cdot d\theta. \end{aligned} \quad (2)$$

Moreover, the coordinate system being object-centered, the decomposition of an object is almost invariant in translation. The effect of the rotation $R(\alpha, \beta, \gamma)$, where α, β and γ are the Euler angles, on the C_l^m coefficients, can be expressed by the relationship:

$$C_l^m(\alpha, \beta, \gamma) = \sum_{n=-l}^{l} D_{mn}^l(\alpha, \beta, \gamma) \cdot C_l^n,$$

where C_l^m and C_l^n respectively are the coefficients before and after the rotation of the shape, and D_{mn}^l is an explicit function of α, β and γ [Burel, 95a]. Burel used these properties in order to register 3D rigid shapes in a direct way.

The computation of the C_l^m coefficients can be performed in two different ways depending on the regularity of the sampling of the surface. The expression of equation (2) in a discrete sum over the sphere allows to compute the coefficients in a simple way. Because the representation is in the form of a linear combination of fixed basis functions, the C_l^m coefficients can also be computed by a conventional least-squares algorithm [Chen, 94] in order to take sparse data into account.

Equation (1) gives the expression of a real function $\Psi(\theta, \varphi)$ in the form of a linear combination of complex spherical harmonics. Nevertheless, can be decomposed into a sum of real functions :

$$\begin{aligned} \Psi(\theta, \varphi) = \sum_{l=0}^{\infty} \Big(& U_l^0 \cdot P_l^0(\cos\theta) \\ & + \sum_{m=1}^{l} (U_l^m \cdot P_l^m(\cos\theta) \cdot \cos\varphi \\ & + V_l^m \cdot P_l^m(\cos\theta) \cdot \sin\phi) \Big). \end{aligned} \quad (3)$$

The total number of coefficients U_l^m and V_l^m, which is the same as the number of C_l^m coefficients (appendix a.3), equals to $(1 + L)^2$, where L is the spatial level of decomposition $(0 \le l \le L)$.

When it comes to the modeling of moving (deformable) non-rigid shapes, the time component has to be introduced. A multiresolution, time-dependent representation is then considered. Time-dependent spherical harmonics are solutions of the wave propagation equation in spherical coordinates. The differential equations in θ and ϕ are equivalent to those expressed in the static case. Details about the separation of the variables are given in [Arfken, 85]. The time dependence is simply achieved by introducing sinusoidal components in equation (3). The time-dependent model is then expressed as follows:

$$\Psi(\theta,\varphi,t)=\sum_{l=0}^{\infty}\sum_{k=0}^{\infty}\Big(Uc_{kl}^{0}\cdot P_l^0(\cos\theta)\cdot\cos\Big(\frac{2\pi kt}{\tau}\Big)$$
$$+Us_{kl}^{m}\cdot P_l^0(\cos\theta)\cdot\sin\Big(\frac{2\pi kt}{\tau}\Big)\cdot(1-\delta_{k0})$$
$$+\sum_{m=1}^{l}\Big(Uc_{kl}^{m}\cdot P_l^m(\cos\theta)\cdot\cos\varphi\cdot\cos\Big(\frac{2\pi kt}{\tau}\Big)$$
$$+Us_{kl}^{m}\cdot P_l^m(\cos\theta)\cdot\cos\varphi\cdot\sin\Big(\frac{2\pi kt}{\tau}\Big)\cdot(1-\delta_{k0})$$
$$+Vc_{kl}^{m}\cdot P_l^m(\cos\theta)\cdot\sin\varphi\cdot\cos\Big(\frac{2\pi kt}{\tau}\Big)$$
$$+Vs_{kl}^{m}\cdot P_l^m(\cos\theta)\cdot\sin\varphi\cdot\sin\Big(\frac{2\pi kt}{\tau}\Big)\cdot(1-\delta_{k0})\Big)\Big),$$

where δ_{k0} is the Kronecker symbol ($\delta_{k0}=1$ for $k=0$, and $\delta_{k0}=0$ for $k\neq 0$), τ is the period of a temporal sequence of surface data and k is a wave number [Matheny, 95]. The maximum value of k (noted K) sets the cut off frequency of the possible motions of the surface in the radial direction. If K is the maximum wave number that we call the temporal level of decomposition, the number of coefficients of this multiresolution and time-dependent model is $(L+1)^2(1+2K)$.

Since the time-dependent model is equivalent to decomposition in the Fourier series of spatial spherical harmonics coefficients, we chose to estimate the coefficients in a two-step algorithm:

1) estimation of the spatial coefficients $U_l^m(t_i)$ and $V_l^m(t_i)$ at each acquisition instant t_i with a classical least-squares algorithm,
2) estimation of the spatio-temporal coefficients from the sets of spatial coefficients computed in step 1,

for $k\in[0,K]$:

$$Uc_{kl}^{m}=\frac{A}{\tau}\cdot\int_0^{\tau}\Big(U_l^m(t)\cdot\cos\Big(\frac{2\pi kt}{\tau}\Big)\Big)\cdot dt$$

$$\text{and } Vc_{kl}^{m}=\frac{A}{\tau}\cdot\int_0^{\tau}\Big(V_l^m(t)\cdot\cos\Big(\frac{2\pi kt}{\tau}\Big)\Big)\cdot dt,$$

for $k\in[1,K]$:

$$Us_{kl}^{m}=\frac{A}{\tau}\cdot\int_0^{\tau}\Big(U_l^m(t)\cdot\sin\Big(\frac{2\pi kt}{\tau}\Big)\Big)\cdot dt$$

$$\text{and } Vs_{kl}^{m}=\frac{A}{\tau}\cdot\int_0^{\tau}\Big(V_l^m(t)\cdot\sin\Big(\frac{2\pi kt}{\tau}\Big)\Big)\cdot dt,$$

with $A=1$ for $k=0$, and $A=2$ for $k\geq 1$.

Relations between the spatial coefficients $U_l^m(t)$ and $V_l^m(t)$ at instant $t\in[0,\tau]$ and the time-dependent coefficients Uc_{kl}^m, Vc_{kl}^m, Us_{kl}^m and Vs_{kl}^m are given in appendix a.4. The results obtained by this method are on the same order of accuracy as those obtained by a global estimation of the time-dependent coefficients with a least-squares algorithm. Nevertheless, the computation time is drastically reduced since it is of the order of the time needed for the inversion of N square matrices of dimension $(L+1)^2$ where N is the number of sample instants t_i in the temporal sequence of period τ (the computation time of the Fourier decomposition being negligible). Moreover, this two-step method allows us to keep the relationship between the spatial characterization of the shape and the spherical harmonics vectors. Below, quantitative results are given in the modeling of the heart left ventricle.

First Application: Modeling and Deformation Analysis of the Vertebra

The diagnosis of scoliotic spine is actually based on measurements (Cobb's Angle) performed from 2D X-ray images. The use of optical images and Moiré techniques could offer some interesting perspectives for the non-invasive detection of scoliosis, but it is still under study

and evaluation [Chalupova, 96]. Digital X-ray's ability to image the complete spine in a natural position [Van Eeuwijk, 97], its low cost, ease of use, and, above all, its low patient irradiation when compared with CT, make it the best suited and standard acquisition device in the examination of scoliosis. Nevertheless, it provides only a 2D projection image of the structure of interest. The 3D information required for an accurate diagnosis of a scoliosis has to be deduced from at least two images, taken under different projection angles, and showing superimposed anatomical shapes. The consideration of an a priori geometrical knowledge can be integrated in order to:

i) solve the 3D reconstruction problem from 2D images by increasing the realism and the accuracy of the recovered shape while reducing the interactive process,

ii) improve the reliability of the diagnosis by comparing custom shapes based parameters with reference parameters,

iii) simulate and guide surgical procedures.

Hence, in a three dimensional approach [Lavaste, 94][Dansereau, 91], the constitution of an elaborate and precise geometrical model of the spine structure is of primary importance for the diagnosis, the understanding and characterization of scoliosis phenomena and the correction of spine disorders. The actual knowledge and classification of non pathological vertebrae allow the constitution of a set of reference shapes, by means of surface models obtained from in-vitro data. The differences between real shapes and reference shapes are mainly given by scale parameters. When it comes to pathological cases, the shape of a vertebra can be seen as the result of different deformations, such as torsion or flexion, applied to a reference shape. In the following section we address the problem of geometrical modeling of the spine, by focusing on the modeling and deformation analysis of the shape of an isolated vertebra described by CT data. We first present the application of spherical harmonics to the modeling of the vertebra surface, then we study the behavior of the model under particular deformations. We especially establish a relationship between some surface coefficients and the deformation parameters. We propose a general framework for the analysis of the deformations or shape characteristics and we show how real deformations encountered in scoliotic phenomena (scale factors, torsion) can be recovered from certain coefficients of the deformed surface model. This framework is a part of the three dimensional approach aimed at a computer aided diagnosis of the scoliotic spine. Our objective at end should be to include, in this scheme, a 3D reconstruction process based on the computation of spherical harmonics coefficients from the patient 2D images.

Vertebra shape modeling

In order to determine the best sampling rate for each shape we analyze the values taken by C_0^0. This coefficient corresponds to the sum of different surface patches resulting from the sampling of the shape. A gradually increasing sampling of the shape provides surface patches of decreasing sizes, hence a convergence of C_0^0 towards an optimal magnitude. The surface points are detected along the rays expressed in a spherical coordinate system. The vertebra being acquired in-vitro, a sub-voxel precision is simply obtained with a trilinear interpolation and a thresholding of the gray level values. In order to be accurately modeled, the input surface has to be star-shaped, that means there is an explicit relationship between the surface and the sphere. Unfortunately, if we consider the highest level of accuracy in the description of the vertebra shape, including the finest details of the vertebral body, pedicles and articular facets, this is not the case.

One solution, when the radius is multiple-valued, is to consider the farthest point from the center of the spherical coordinate system. Since the object surface is approximated by its star-shaped envelope, shape features such as cavities, tunnels or overhangs can be lost. The problem of modeling non star- shaped objects with spherical harmonics, by a parametrization that establishes a one to one mapping from the original object surface to the unit sphere, has been addressed in [Brechbüler, 95]. Here we adopt an alternative solution, and that is to partition the initial volume image with respect to anatomical features, such as pedicles, in order to decompose the original object into star-shaped sub-objects. Figure 2 shows a shaded polygons representation of the original data as well as the modeling of the vertebral body and articular facets with spherical harmonics at various resolution levels. The surface data was obtained

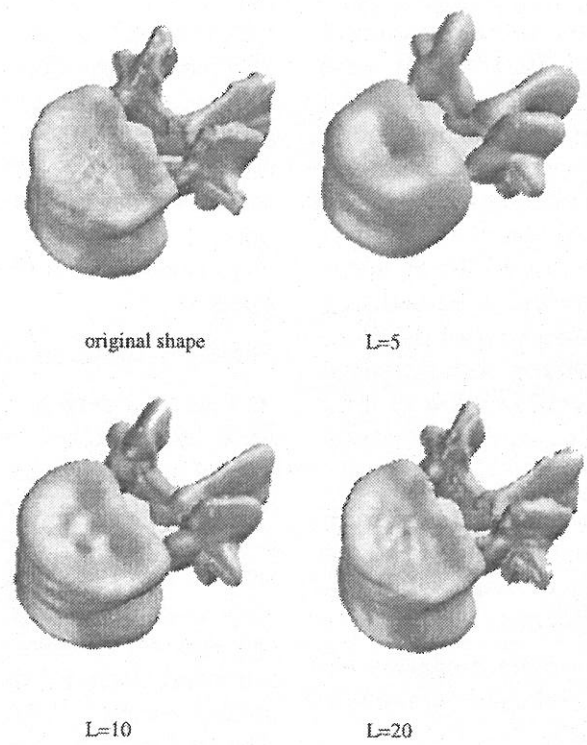

Fig. 2. Modeling of a complete lumbar vertebra with spherical harmonics.

from a $102 \times 256 \times 256$ CT image of an *in-vitro* lumbar vertebra. The volume image was previously partitioned by means of separating planes, empirically defined, and processed (surface detection) in order to constitute four sets of 3280 surface points. The mean error between the surface model and the sampling points is about 1.27 per cent (mean error of 0.64 voxel for a mean radius value of 50 voxels) at the decomposition level $L = 20$ (441 coefficients).

Deformation analysis

We study the behavior of the model with respect to particular deformations. If we consider a reference shape (*a priori* knowledge) on which deformations have been applied, we can show how it is possible to estimate these deformations from spherical harmonics coefficients of the deformed surface (a pathological shape for instance). This process is based on a preliminary deformation of the reference shape and the estimation of the variation laws of some coefficients of the model under deformations (Figure 3). The variation laws are estimated only once in the analysis step to complete the a priori knowledge on the shape. Three scale deformations along the cartesian axes and the torsion along one axis are considered. It is then possible to compute the deformations (scale and torsion), between an unknown shape S_u and the reference shape S_r, from the deformation laws associated with particular C_l^m coefficients. The consideration of the other C_l^m coefficients allows us to determine whether the two shapes are different in terms of the considered deformations.

Deformations are applied during the detection of the 3D surface points of the reference shape. The scale deformations are defined as scale factors applied along the three axes of the cartesian coordinate system $\mathbf{R}^3(X, Y, Z)$ of the shape:

$$\begin{cases} x = a_x \cdot R \cdot \sin\theta \cdot \cos\varphi, \\ y = a_y \cdot R \cdot \sin\theta \cdot \sin\varphi, \\ z = a_z \cdot R \cdot \cos\theta, \end{cases}$$

where a_x (respectively a_y, a_z) corresponds to a deformation along the X axis (respectively Y, Z axis) and θ, φ, R are the coordinates of the 3D surface points in the spherical coordinate system. In the same way, a torsion along the Z axis has been considered. The coordinates (x, y, z) of the reference shape are transformed

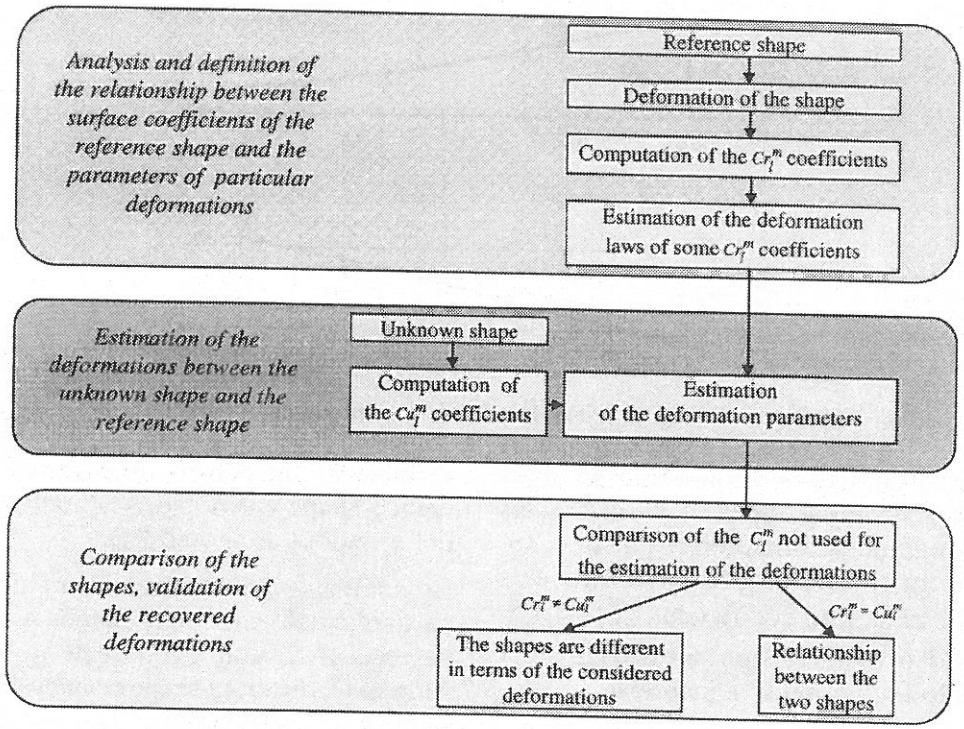

Fig. 3. Deformation analysis flowchart.

as follows:

$$\begin{cases} x' = x \cdot \cos t_z - y \cdot \sin t_z \\ y' = x \cdot \sin t_z + y \cdot \cos t_z \\ z' = z. \end{cases}$$

The angle t_z is expressed with respect to the z coordinate:

$$t_z = t \cdot \frac{z - z_{\min}}{z_{\max} - z\min}$$

where $z_{\min}$ and $z_{\max}$ are the limit values of z and t is a constant torsion angle between $z_{\min}$ and $z_{\max}$.

Different values of the scale parameters a and the torsion parameter t have been applied to the reference shape in the following way:

$$\begin{aligned} &a_x = \text{variable} \;\; a_y = 1.0 \;\; a_z = 1.0 \;\; t = 0, \\ &a_x = 1.0 \;\; a_y = \text{variable} \;\; a_z = 1.0 \;\; t = 0, \\ &a_x = 1.0 \;\; a_y = 1.0 \;\; a_z = \text{variable} \;\; t = 0, \\ &a_x = 1.0 \;\; a_y = 1.0 \;\; a_z = 1.0 \;\; t = \text{variable}. \end{aligned}$$

$a = 1$ means that there is no deformation, whereas $a < 1$ corresponds to an expansion of the shape, and $a > 1$ to a compression of the shape. For each of these deformations the coefficients have been computed up to the order $L = 4$. Figure 4 gives two examples of the deformation curves $C_l^m = f(a)$ obtained on C_0^0 and C_4^0 respectively, for a variation of the scale parameter $a_x(0.6 < a_x < 1.4)$ and a variation of the scale parameter $a_z(0.6 < a_z < 1.4)$.

A linear approximation being insufficient to take into account the stronger deformations, the deformation curves $C_l^m = f(\delta)$, where δ is the deformation parameter, are estimated with polynomial equations. We can thus write:

$$C_l^m(\delta) = a \cdot (\delta - \delta_0)^2 + b \cdot (\delta - \delta_0) + c,$$

where a, b, c are the parameters of the deformation curves and $c = Cr_l^m$ is the coefficient of the reference shape obtained for $\delta = \delta_0$ (the null deformation).

The correction to apply to a coefficient Cu_l^m of an unknown shape, in order to recover the coefficient Cr_l^m of the reference shape, is given by the following equation:

$$\begin{aligned} -\Delta(\delta) &= Cu_l^m(\delta) - Cr_l^m \\ &= a(\delta - \delta_0)^2 + b(\delta - \delta_0), \end{aligned}$$

where δ is the unknown parameter (a_x, or a_y, or a_z, or t), This non-linear equation can be

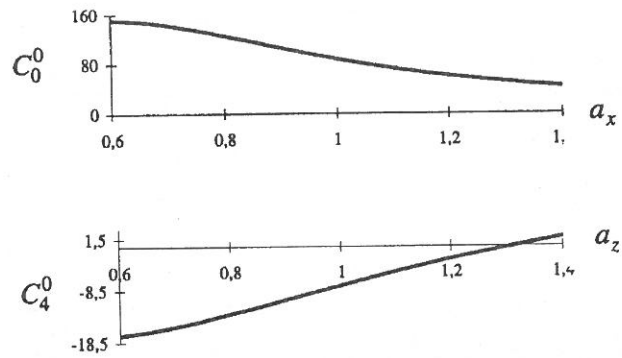

Fig. 4. Examples of deformation curves.

solved with a standard Newton–Raphson algorithm. When different types of deformations are considered, the deformation parameters are estimated from several couples of coefficients (Cu_l^m, Cr_l^m). First, four coefficients C_0^0, C_1^0, C_2^0, C_4^0 (independent of the torsion) are used in order to form the following set of equations:

$$\begin{aligned} Cu_0^0 - Cr_0^0 &= \Delta(a_x) + \Delta(a_y) + \Delta(a_z), \\ Cu_1^0 - Cr_1^0 &= \Delta(a_x) + \Delta(a_y) + \Delta(a_z), \\ Cu_2^0 - Cr_2^0 &= \Delta(a_x) + \Delta(a_y) + \Delta(a_z), \\ Cu_4^0 - Cr_4^0 &= \Delta(a_x) + \Delta(a_y) + \Delta(a_z), \end{aligned}$$

where a_x, a_y, and a_z are the unknown scale parameters. The torsion parameter t is then computed by considering the equation given by the imaginary part of coefficient C_4^4:

$$Cu_4^4 - Cr_4^4 = \Delta(a_x) + \Delta(a_y) + \Delta(a_z) + \Delta(t).$$

The results obtained on the vertebral body of the lumbar vertebra, deformed with the three scale parameters and a torsion parameter, are reported in Table 1. The deformations applied to the reference shape are noted AD and the recovered deformations are noted RD.

		a_x	a_y	a_z	t
test 1	AD	0.8	0.8	1.2	0°
	RD	0.82	0.78	1.21	−0.374°
test 2	AD	1.2	0.8	1.2	4°
	RD	1.17	0.86	1.18	4.15°
test 3	AD	0.8	1.2	1.2	4°
	RD	0.80	1.23	1.19	4.02°
test 4	AD	0.8	1.2	0.8	16°
	RD	0.8	1.22	0.79	15.1°

Table 1. Deformation tests

By analyzing the coefficients of the modeling, particular deformations between two shapes can be recovered with a relatively good accuracy. Moreover, different shapes can be discriminated in terms of the considered deformations. Other types of deformations such as flexion as well as rigid transformations (rotation, translation) have now to be introduced into the equations, in order to improve the discrimination and the characterization of the shapes. Furthermore, we intend to constitute a complete model of the spine in order to provide an a priori geometrical knowledge for the diagnosis of spine scoliosis in a three-dimensional approach (reconstruction from 2D images). Consideration of the complete spine structure should be of primary interest understanding and analyzing the evolution of vertebra shapes along the spine.

Second Application: Dynamic Modeling of the Left Ventricle Cavity

The characterization of the left ventricle shape and motion is of main concern in the diagnosis of heart diseases. We present here an application of spherical harmonics to the modeling of a clinical SPECT data sequence.

The temporal sequence is composed of SPECT data sets ($64 \times 64 \times 64$) acquired at different instants of the cardiac cycle. The acquisition was synchronized on the ECG signal (end systole). The data sets have been reconstructed with a filtered backprojection algorithm (Hahn filter). In the clinical procedure, the data is oriented in the volume image so that the principal axis of

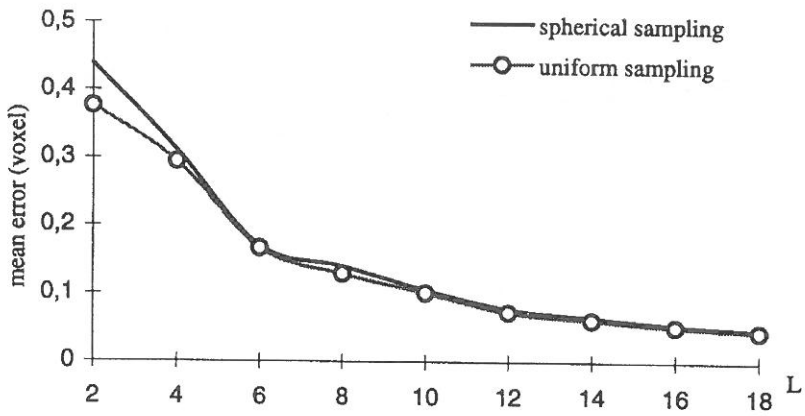

Fig. 5. Effect of the surface sampling on the model accuracy for different values of L.

the cavity is parallel to one axis of the volume image at instant $t = 0$. The segmentation of SPECT volumes of the temporal sequence provides the input data. The 3D surface points of the ventricle cavity are detected along the rays expressed in a spherical coordinate system, the detection is based on a trilinear interpolation and a thresholding. In order to take into account temporal dependence between the data sets, the threshold at instant t is fixed at a percentage P of the mean value of the maxima of smoothed histograms at instants $t-1$ and $t+1$. P has been determined according to subjective criteria and has been fixed at 50 percent. In order to get a closed surface of the ventricle cavity, a separation plane between the ventricle cavity and the aorta is arbitrarily defined.

A classical sampling of smoothed closed surfaces is obtained by a description of the definition domain of angular spherical coordinates (θ, φ) by constant steps $\Delta\theta, \Delta\varphi$. This type of sampling leads to significant differences on the patch surfaces between the regions close to the equator and the regions close to the poles of the sphere. For this reason, we have tested a more uniform sampling [Foley, 90] based on the subdivision of the triangular faces of the tetrahedron with vertices on the unit sphere. Accuracy of the modeling of the left ventricle at instant $t = 0$ is given in Figure 5 for the two types of sampling, i.e., spherical and almost uniform sampling. The mean error between the original data and the spatial model is slighter with the sampling almost uniform, and obviously decreases, in both cases, with the spatial level of decomposition L.

As mentioned before, spatial coefficient vectors are first estimated independently, by a least-squares algorithm, from the sets of 3D surface points. The time-dependent coefficients of the model are then computed by the decomposition in the Fourier series of each component of the static spherical harmonics vectors. The influence of the temporal order of decomposition K on the accuracy of a time-dependent modeling based on spherical harmonics as well as on a modeling based on the spheroidal harmonics is shown in Figure 6. One can note that the results obtained with spheroidal harmonics are on the same order of magnitude as those obtained with spherical harmonics.

With a spatial level of decomposition $L = 10$ and a temporal level of decomposition $K = 5$, the mean error between the original data and the time-dependent model is around 0.15 voxel. A shaded polygon representation (Figure 7) illustrates the results of the modeling at 16 different instants of the cardiac cycle. The computation time on a Pentium PC 100 MHz of each spherical harmonics vector is less than 1 s for $L = 2$ (9 parameters) and 16 s for $L = 10$ (121 parameters). Thus, the computation time with the two-steps algorithm is of the order of the computation time of 16 spatial spherical harmonics vectors, i.e., 256 s for $L = 10$ and $K = 5$, whereas the time needed for a global computation of the time-dependent spherical harmonics vector for $L = 5$ and $K = 3$ is of 1200 s.

The ejection fraction is an important parameter for the actual characterization of the left ventricle function. The temporal evolution of the

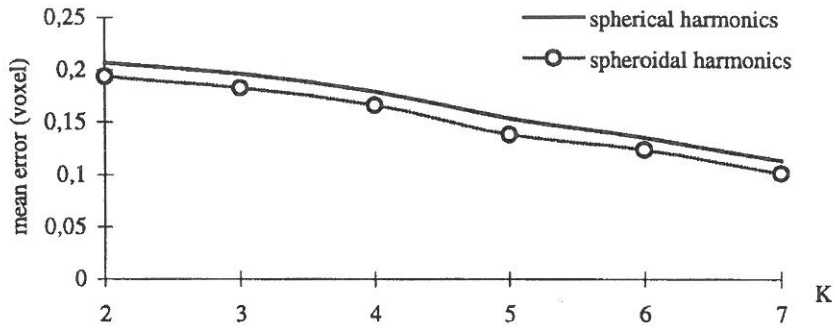

Fig. 6. Comparison of spherical harmonics and spheroidal harmonics for different values of K.

ejection fraction is defined as follows:

$$EF(t) = \frac{V(t) - V_{ES}}{V_{ED}},$$

where $V(t)$ is the volume of the left ventricle cavity at instant t, V_{ES} is the minimum volume of the left cavity (end systole, $t_i = 5$), and V_{ED} is the maximum volume of the left cavity (end diastole). The behavior of the ejection fraction $EF(t)$ for a static modeling of the 16 independent volume images and for a time-dependent modeling with two levels of temporal decomposition ($K = 4, K = 5$) is given in Figure 8.

The modeling of 3D SPECT data with spherical harmonics provides instantaneous values of the cavity volume, and thus, an accurate quantification of the ejection fraction. The result obtained is consistent with the one expected in a healthy patient. It still has to be validated in several pathological and non pathological cases. Moreover, it is interesting to compare evolution of the ejection fraction with the evolution of the first coefficient of the time-dependent model $U_0^0(t)$ (Figure 9).

Beyond the computation of features such as the ejection fraction, the properties of this accurate time-dependent model offer some interesting perspectives to characterize the ventricle shape and motion, and to register and reconstruct volume data sets.

Conclusion

We have accurately depicted a multiresolution representation based on spherical harmonics for the modeling of complex static anatomical shapes, illustrated by the vertebra, and of non-rigid moving (deformable) shapes, illustrated by the endocardial surface. We have shown that some spatial and time- varying features of the shapes could be quantified from the model coefficients with a relatively good accuracy. For diagnostic purposes, more elaborate relationships between the shape features and the model coefficients still have to be brought out and introduced in this analysis, in order to improve the discrimination and the characterization of anatomical shapes. Furthermore, spherical harmonics offer some interesting perspectives in helping to register and reconstruct 3D anatomical shapes. Thus, spherical harmonics can be appropriate for the analysis and the computation of transformations between 3D surfaces. Nevertheless, even if particular transformations can be deduced from some coefficients of the model, the inverse problem, i.e. computing the effect of a given transformation on all the model coefficients (in order to fit the data) still remains a problem that needs to be solved.

Appendix

a.1. Laplace's equation

The Laplace's equation in a spherical coordinate system (where r, θ and φ are the spherical coordinates) is:

$$\frac{\partial}{\partial r}\left(r^2 \frac{\partial F}{\partial r}\right) + \frac{1}{\sin\theta}\frac{\partial}{\partial \theta}\left(\sin\theta \frac{\partial F}{\partial \theta}\right) + \frac{1}{\sin^2\theta}\frac{\partial^2 F}{\partial \varphi^2} = 0.$$

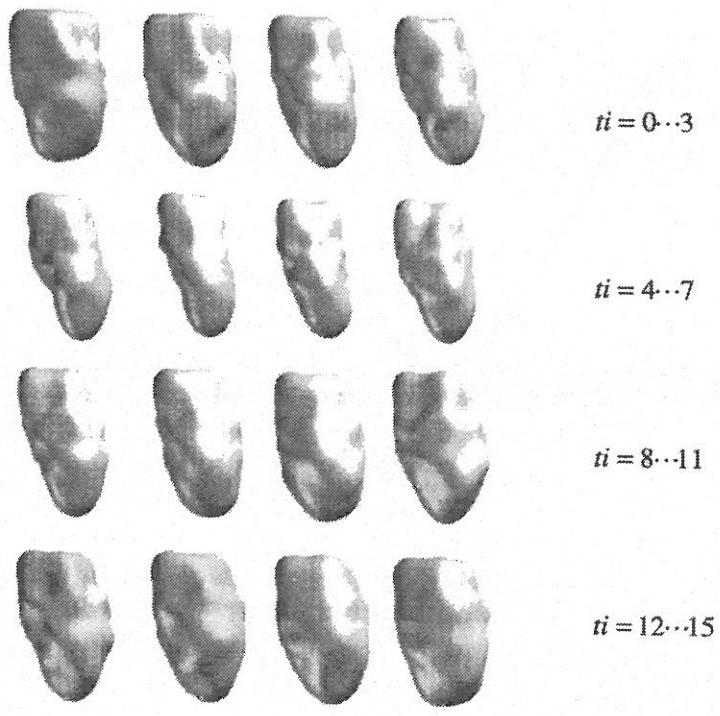

Fig. 7. Time-dependent modeling of the left ventricle cavity ($L = 10, K = 5$).

a.2. Spherical Harmonics

Spherical harmonics are the solutions of Laplace's equation in spherical coordinates:

$$\begin{cases} Y_l^m(\theta, \varphi) = (-1)^m \cdot N_l^m \cdot P_l^m(\cos\theta) e^{im\varphi} \\ \qquad\qquad \text{for } l \geq 0 \text{ and } 0 \leq m \leq l, \\ Y_l^m(\theta, \varphi) = (-1)^m \left(Y_l^{-m}(\theta, \varphi)\right)^* \\ \qquad\qquad \text{for } l > 0 \text{ and } -l \leq m \leq 0, \end{cases}$$

where * denotes the complex conjugate,

$N_l^m = \sqrt{\dfrac{2l+1}{4\pi}} \cdot \sqrt{\dfrac{(l-m)!}{(l+m)!}}$ are normalization constants,

$P_l^m(u) = (-1)^m \cdot (1-u^2)^{\frac{m}{2}} \cdot \dfrac{d^m}{du^m} P_l(u)$ are the associated Legendre Polynomials,

and $P_l(u) = \dfrac{1}{2^l \cdot l!} \cdot \dfrac{d^l}{du^l}(1-u^2)^l$ are the Legendre polynomials.

a.3. Coefficients of the spherical harmonics decomposition

The C_l^m coefficients are related to U_l^m and V_l^m real coefficients in the following way:

$$U_l^0 = \mathrm{Re}\,(C_l^0) \cdot N_l^0, \quad N_l^m = \sqrt{\frac{2l+1}{4\pi}} \cdot \sqrt{\frac{(l-m)!}{(l+m)!}},$$

$$U_l^m = 2 \cdot \mathrm{Re}\,(C_l^m) \cdot (-1)^m \cdot N_l^m \text{ for } 1 \leq m \leq l,$$

$$V_l^m = -2 \cdot \mathrm{Im}\,(C_l^m) \cdot (-1)^m \cdot N_l^m \text{ for } 1 \leq m \leq l.$$

a.4. Relations between spatial coefficients and time-dependent coefficients

The spatial components of a spherical harmonics vector at instant $t \in [0, \tau]$ are:

$$U_l^m(t) = \sum_{k=0}^{K} \left(Uc_{kl}^m \cdot \cos\left(\frac{2\pi kt}{\tau}\right) + Us_{kl}^m \cdot \sin\left(\frac{2\pi kt}{\tau}\right) \cdot (1 - \delta_{k0}) \right) \quad \forall m, \text{ an integer such as } 0 \leq m \leq l,$$

$$V_l^m(t) = \sum_{k=0}^{K} \left(Vc_{kl}^m \cdot \cos\left(\frac{2\pi kt}{\tau}\right) + Vs_{kl}^m \cdot \sin\left(\frac{2\pi kt}{\tau}\right)(1 - \delta_{k0}) \right) \quad \forall m, \text{ an integer such as } 0 < m \leq l,$$

where δ_{k0} is the Kronecker symbol.

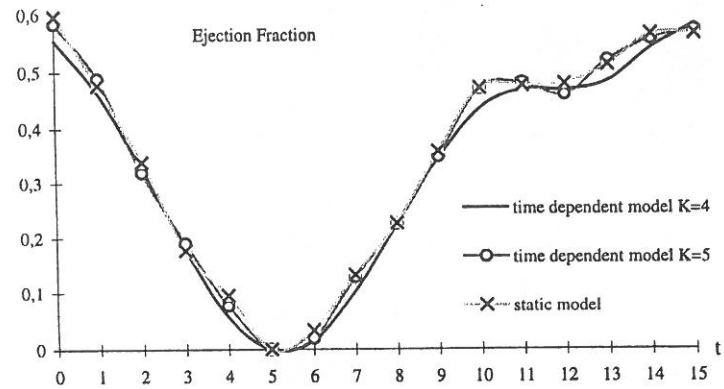

Fig. 8. Ejection fraction, ($L = 10$).

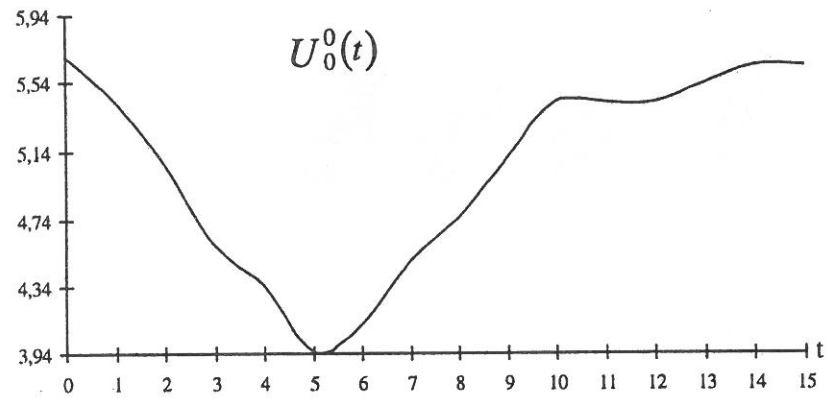

Fig. 9. Evolution of $U_0^0(t)$.

Acknowledgments

The authors would like to acknowledge Prof. Dr. A. Ramée, Prof. Dr. R. Duvauferrier, Dr. Y. Rolland at the Département de Radiologie et d'Imagerie Médicale, CHRU de Rennes (France), and Prof. P. Bourguet and Dr. A. Devillers at Centre Eugène Marquis, CHRU de Rennes (France), and I. Stanghellini for their contributions.

References

G. ARFKEN, (1985) Mathematical methods for physicists, Third edition, New York : academic press.

E. BARDINET ET AL., (1996) Tracking medical 3D data with a deformable parametric model, Presented at Proceedings of the European Conference of Computer Vision , EECV 96, April 14–18, Cambridge, England.

R. M. BOLLE AND B. C. VEMURI, (1991) On three-dimensional surface reconstruction methods, IEEE Transactions on Pattern Analysis and Machine Intelligence, 13, 1, 1–13.

F. L. BOOKSTEIN, (1989) Principal warps : thin-plate splines and the decomposition of deformations, IEEE Transactions on Pattern Analysis and Machine Intelligence , 11, 6, 567–585.

CH. BRECHBÜLER ET AL., (1995) Parametrization of closed surfaces for 3D shape description, Computer vision and image understanding, 61, 2, 154–170.

G. BUREL AND H. HENOCQ, (1995) Three-dimensional invariants and their application to object recognition, Signal Processing, 45, 1–22.

G. BUREL AND H. HENOCQ, (1995) Determination of the orientation of 3D objects using spherical harmonics, Graphical Models and Image Processing, 57, 5, 400–408.

M. CHALUPOVA AND D. VALOVA, (1996) Evaluation of exercises effect by moire technology, Presented at Proceedings of the 13th Biennial International Conference Biosignal'96, June 1996, Brno, Czech Republic.

C. W. CHEN ET AL., (1994) Modeling, analysis, and visualization of left ventricle shape and motion by hierarchical decomposition. IEEE Transactions on Pattern Analysis and Machine Intelligence, 16, 4, 342–356.

J. L. COATRIEUX ET AL., (1996) From algorithm to applications in medical imaging : present and future, Presented at Eurographics'96, State of the Art reports, Poitiers, France.

J. DANSEREAU, (1991) Evaluation of the immediate effect of the boston on scoliotic deformity by means of spinal and rib cage 3D reconstruction, Presented at Proceedings of the 37th meeting of the ORS, 2.

T. DEROSE ET AL., (1995) Multiresolution analysis of arbitrary meshes, Technical report of Department of Computer Science and Engineering, University of Washington, January.

T. A. FOLEY ET AL., (1990) Visualizing functions over a sphere, IEEE Computer Graphic & Applications, 1, 32–40.

W. FREEDEN AND U. WINHEUSER, (1995) Combined spherical harmonic and wavelet expansion, Report of University of Kaiserlautern, Laboratory of Technomathematics, Geomathematics group, Germany.

F. LAVASTE ET AL., (1992) 3D geometrical and mechanical modeling of the human lumbar spine, Journal of Biomechanics, 25, 10, 1153–1164.

A. MATHENY AND D. GOLDGOF, (1995) The use of three and four dimensional surface harmonics for rigid and nonrigid shape recovery and representation, IEEE Transactions on Pattern Analysis and Machine Intelligence, 17, 10, 967–981.

L. N. MAX AND E. D. GETZOFF, (1988) Spherical harmonic molecular surfaces, Computer Graphics & Applications, 7, 42–50.

T. MCINERNEY AND D. TERZOPOULOS, (1996) Deformable models in medical image analysis: a survey, Medical Image Analysis, Oxford University Press, 1, 2, 91–108.

A. PENTLAND AND B. HOROWITZ, (1991) Recovery on nonrigid motion and structure, IEEE Transactions on Pattern Analysis and Machine Intelligence, 13, 7, 730–742.

J. SEQUEIRA ET AL., (1992) Three-dimensional modeling of tree-like anatomical structure, in 3D advanced image processing in medicine, Presented at Proceedings of the 14th IEEE EMBS conference Satellite Symposium, edited by C. Roux, G. T. Herman, R. Collorec.

F. SOLINA AND R. BAJCSY, (1990) Recovery of parametric models from range images : the case for superquadrics with global deformations, IEEE Transactions on Pattern Analysis and Machine Intelligence, 12, 2, 131–147.

A. H. W. VAN EEUWIJK ET AL., (1997) A novel method for digital X-ray imaging of the complete spine, Philips Medical Systems, Presented at CVRMed–MRCAS'97, Grenoble, France.

Received: June, 1997
Revised: May, 1998
Accepted: May, 1998

Contact address:
P. Haigron
Laboratoire de Traitement du Signal et de l'Image, INSERM
Université de Rennes 1
Bât. 22, Campus de Beaulieu
35042 Rennes Cedex
France
phone: 33 (0)2 99 28 69 19
fax: 33 (0)2 99 28 69 17 email:
pascal.haigron@univ-rennes1.fr

PASCAL HAIGRON received the DEA in Instrumentation and Control, Caen, France, 1989. In June 1993, he completed his Ph.D. in signal processing and telecommunications, and he is currently Maître de Conférences at the University of Rennes 1, France. His research interests are in 3–D medical imaging.

GILDAS LEFAIX received the DEA in Image Processing from the University of Rennes 1, France, in 1996. Since October 1996 he is a Ph.D. student at the LTSI (Signal and Image Processing Laboratory), University of Rennes 1, France. His research interests include 3D shape modeling and medical image processing.

XAVIER RIOT received the DEA in signal processing in 1992, and he completed his Ph.D. in signal processing and telecommunications in December 1998, at the University of Rennes 1, France. Since January 1994, he is engineer at Hexale Technologies. His research interests include telemedicine and 3D medical imaging.

RENÉ COLLOREC received the Habilitation à Diriger des Recherches in 1988. He is Professor at the University of Rennes 1, France, and Head of the Diplôme d'Etudes Approfondies (DEA) in Telecommunications, Image, Signal, Radar, of the University of Rennes 1. His research interests are in image processing with medical applications.